

Article

## Systematic Study of Binding of $\mu$ -Conotoxins to the Sodium Channel Na<sub>V</sub>1.4

Somayeh Mahdavi and Serdar Kuyucak \*

School of Physics, University of Sydney, Sydney, New South Wales 2006, Australia;

E-Mail: Sahar@physics.usyd.edu.au

\* Author to whom correspondence should be addressed; E-Mail: serdar@physics.usyd.edu.au;

Tel.: +61-29-036-5306.

External Editor: Jean-Marc Sabatier

Received: 7 November 2014; in revised form: 1 December 2014 / Accepted: 10 December 2014 /

Published: 18 December 2014

---

**Abstract:** Voltage-gated sodium channels (Na<sub>V</sub>) are fundamental components of the nervous system. Their dysfunction is implicated in a number of neurological disorders, such as chronic pain, making them potential targets for the treatment of such disorders. The prominence of the Na<sub>V</sub> channels in the nervous system has been exploited by venomous animals for preying purposes, which have developed toxins that can block the Na<sub>V</sub> channels, thereby disabling their function. Because of their potency, such toxins could provide drug leads for the treatment of neurological disorders associated with Na<sub>V</sub> channels. However, most toxins lack selectivity for a given target Na<sub>V</sub> channel, and improving their selectivity profile among the Na<sub>V</sub>1 isoforms is essential for their development as drug leads. Computational methods will be very useful in the solution of such design problems, provided accurate models of the protein-ligand complex can be constructed. Using docking and molecular dynamics simulations, we have recently constructed a model for the Na<sub>V</sub>1.4- $\mu$ -conotoxin-GIIIA complex and validated it with the ample mutational data available for this complex. Here, we use the validated Na<sub>V</sub>1.4 model in a systematic study of binding other  $\mu$ -conotoxins (PIIIA, KIIIA and BuIIIIB) to Na<sub>V</sub>1.4. The binding mode obtained for each complex is shown to be consistent with the available mutation data and binding constants. We compare the binding modes of PIIIA, KIIIA and BuIIIIB to that of GIIIA and point out the similarities and differences among them. The detailed information about Na<sub>V</sub>1.4- $\mu$ -conotoxin interactions provided here will be useful in the design of new Na<sub>V</sub> channel blocking peptides.

**Keywords:** sodium channels; conotoxins; homology modeling; docking; molecular dynamics; potential of mean force; binding free energy

---

## 1. Introduction

Voltage-gated sodium ( $\text{Na}_V$ ) channels are membrane proteins that are responsible for the excitation of cells in many organs from the nervous system to heart and muscles [1]. Dysfunction of  $\text{Na}_V$  channels is associated with several disorders, such as neuropathic, cardiac and muscular diseases [2]. Blockers of sodium channels from venomous animals, in particular  $\mu$ -conotoxins from cone snails, have been proposed for the treatment of these diseases [3–5].  $\mu$ -conotoxins provide a rich library of peptide blockers of  $\text{Na}_V$  channels, exhibiting a diverse range of affinities for various  $\text{Na}_V1$  isoforms [6]. For example, KIIIA has the highest affinity for  $\text{Na}_V1.2$  among all  $\text{Na}_V1$  isoforms and, hence, could be a candidate for the treatment of neuropathic disorders [7,8]. Similarly, among all  $\mu$ -conotoxins, KIIIA is the most potent blocker of  $\text{Na}_V1.7$ , which is a target for the treatment of chronic pain [9]. Likewise, BuIIIB has a higher affinity for  $\text{Na}_V1.3$  and may be developed as an analgesic [5]. In order to develop  $\mu$ -conotoxins further as drug candidates, their affinity and selectivity profiles for the targeted  $\text{Na}_V1$  isoform need to be improved. Several attempts have been made in this direction, focusing in particular on derivatives of KIIIA [10–15]. However, in the absence of structures for  $\text{Na}_V$  channels, it has been difficult to make progress.

Before their potential for drug development was recognized,  $\mu$ -conotoxins were used extensively in experimental studies of the pore domain of  $\text{Na}_V1$  channels [16–19]. For example, there are plenty of mutation data on binding of  $\mu$ -conotoxins to  $\text{Na}_V1$  channels, which could be exploited to improve the affinity and selectivity properties of  $\mu$ -conotoxins targeting a specific  $\text{Na}_V1$  isoform. Unfortunately, due to the complexity of the binding modes, it has been difficult to uniquely interpret such mutation data, so they have been of limited use in solving the design problems posed by  $\mu$ -conotoxins.

The recent determination of the crystal structures for bacterial  $\text{Na}_V$  channels should help to ameliorate this situation [20–24], provided accurate homology models of mammalian  $\text{Na}_V$  channels could be constructed from the bacterial counterparts. This task is not as straightforward as in potassium channels, because in going from bacterial to mammalian  $\text{Na}_V$  channels: (i) the tetrameric symmetry is lost; (ii) the selectivity filter is not conserved; and (iii) there are no good templates for the linker sequences in the turret region, which widely differs among the four domains. Nevertheless, for precisely the same reasons, crystal structures of mammalian  $\text{Na}_V$  channels are unlikely to be solved in the near future, leaving homology modeling as the best alternative for progress. It will be of crucial importance in such quests to make judicious use of the wealth of functional data available on mammalian  $\text{Na}_V$  channels, both to constrain and to validate the constructed homology models. For this reason, initial efforts have focused on modeling of  $\text{Na}_V1.4$  channel, as a great deal of functional data is available for this channel. These studies include binding of tetrodotoxin [25,26] and  $\mu$ -conotoxins [27–29] to the  $\text{Na}_V1.4$  channel.

Previously, we constructed a model of  $\text{Na}_V1.4$  using the crystal structure of the bacterial  $\text{Na}_V\text{Ab}$  channel and studied the binding of  $\mu$ -conotoxin GIIIA to  $\text{Na}_V1.4$  [29]. This choice was motivated by

the fact that Na<sub>V</sub>1.4-GIIIA was the most studied complex experimentally, offering plenty of functional and mutagenesis data for validating the complex model. Here, we use the validated Na<sub>V</sub>1.4 model to present a systematic study of other  $\mu$ -conotoxins that have therapeutic potential, namely, PIIIA [30], KIIIA [31] and BuIIIB [32]. The channel-toxin complexes are created using docking followed by refinement in molecular dynamics (MD) simulations. This method has been used in the description of potassium channel toxins previously and shown to yield accurate complex structures [33–39]. The Na<sub>V</sub>1.4- $\mu$ -conotoxin complexes obtained are validated by comparing the binding modes to available mutation data. In the case of PIIIA, we also calculate the binding free energy and compare it to the experimental value. Comparison of the binding modes for PIIIA, KIIIA and BuIIIB to that of GIIIA reveals a common scaffold in binding of the four  $\mu$ -conotoxins to Na<sub>V</sub>1.4. The systematic study of the binding modes of  $\mu$ -conotoxins presented here will be valuable in the design of peptide analogs targeting a specific Na<sub>V</sub>1 isoform with enhanced affinity and selectivity properties.

## 2. Computational Methods

Here, we briefly discuss the computational methods used in obtaining the channel-toxin complex structures and the binding free energies of toxins. For details of the methods, we refer to our previous work on toxin binding to sodium [29] and potassium channels [33–39].

### 2.1. Structures of Na<sub>V</sub>1.4 and $\mu$ -Conotoxins

The model for the Na<sub>V</sub>1.4 channel is taken from a previous study [29], where a homology model was constructed using the Na<sub>V</sub>Ab crystal structure [20]. This Na<sub>V</sub>1.4 model was validated by comparing the binding mode and binding free energy results obtained for the Na<sub>V</sub>1.4-GIIIA complex to the available mutagenesis data and the experimental binding free energy [29]. In the following, we will use the binding mode results for the Na<sub>V</sub>1.4-GIIIA complex as a reference in order to facilitate comparison of the binding modes for  $\mu$ -conotoxins PIIIA, KIIIA and BuIIIB,

The alignment diagram for the four  $\mu$ -conotoxins is shown in Figure 1. The three basic residues that are identified as most the significant contributors to the binding of GIIIA to Na<sub>V</sub>1.4 (R13, K16 and R19) are highlighted in blue. To see whether these basic residues are likely to contribute to the binding modes PIIIA, KIIIA and BuIIIB with Na<sub>V</sub>1.4, we superpose their structures with that of GIIIA (Figure 2). The NMR structures of GIIIA [43], PIIIA [44], KIIIA [45] and BuIIIB [42] are taken from the Protein Data Bank with the following respective IDs: 1TCJ, 1R9I, 2LXG and 2LO9. We align the backbone atoms of the C10-Q18 residues in GIIIA with the corresponding ones in PIIIA and KIIIA by minimizing their RMSD. Because there is a gap in BuIIIB at the position of D12, alignment in this case is restricted to the R13-Q18 residues in GIIIA. The R13 and K16 side chains in GIIIA interact with the EEDD ring in Na<sub>V</sub>1.4 and are responsible for the blocking of the pore [29]. We have, therefore, explicitly indicated the R13 and K16 side chains in GIIIA and the corresponding ones in PIIIA, KIIIA and BuIIIB in Figure 2. It is seen that there is a very good overlap between the three  $\mu$ -conotoxins and GIIIA at the binding interface, including the pore blocking R13 and K16 residues in GIIIA. These figures are highly suggestive that all four  $\mu$ -conotoxins may share a common binding motif.

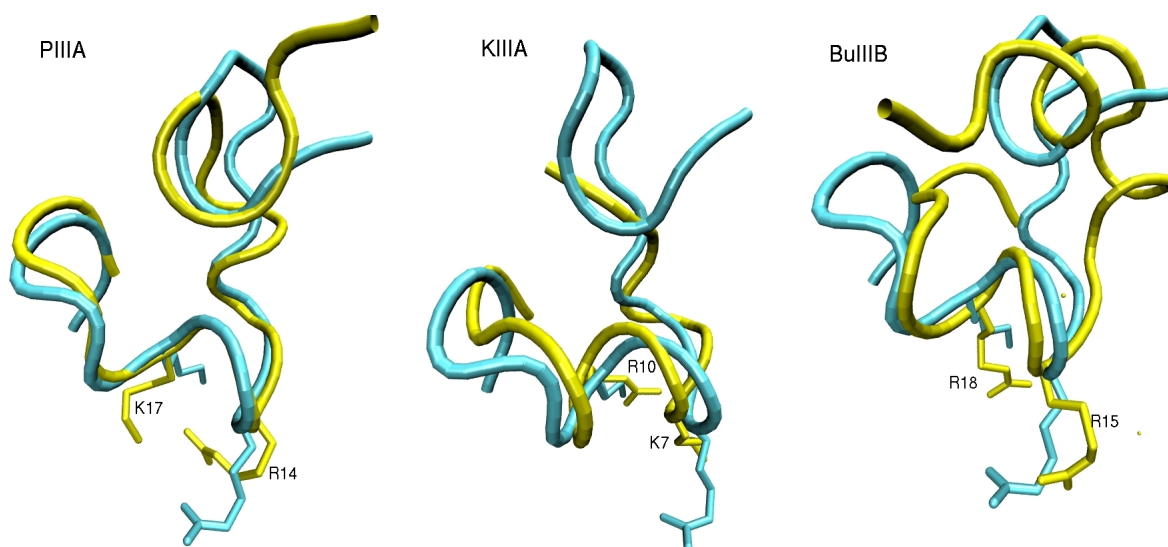
**Figure 1.** Alignment diagram for the  $\mu$ -conotoxins considered in this study. The Cys residues involved in disulfide bridges are shown in yellow, and the Arg and Lys residues that strongly interact with the channel residues in GIIIA are highlighted in blue. The disulfide bridge pattern for the major isomer is assumed in each case, which is 1–4/2–5/3–6 for PIIIA [40] and BuIIIB [42] and 1–5/2–4/3–6 for KIIIA [41]. The star indicates that the C-terminal is amidated.

```

GIIIA  --RDCCTOOKK-CKDRQCKOQ-RCCA*
PIIIA  -ZRLCCGFOKS-CRSRQCKOH-RCC-*
KIIIA  ----CCN-----CSSKWCRDHSRCC-*
BuIIIB VGERCCKNGKRGCG-RWCRDHSRCC-*

```

**Figure 2.** The structures of PIIIA, KIIIA and BuIIIB (yellow) are superposed with that of GIIIA (blue). The side chains of the pore blocking residues R13 and K16 in GIIIA point downward. The corresponding residues in PIIIA (R14 and K17), KIIIA (K7 and R10) and BuIIIB (R15 and R18) are explicitly indicated.



## 2.2. Complex Structures from Docking and MD Simulations

We generate the initial poses for the  $\text{Na}_v1.4$ - $\mu$ -conotoxin complexes using the docking program, HADDOCK [46,47], which has given good results in previous studies of toxin binding to sodium and potassium channels [29,33–39]. HADDOCK works best when some experimental data are applied as restraints in docking. Unfortunately, unlike GIIIA, there are limited mutagenesis data available for binding of PIIIA and KIIIA to  $\text{Na}_v1.4$  (see Table 1) and none for BuIIIB. We will, therefore, use the binding mode for GIIIA as a guide in docking PIIIA, KIIIA and BuIIIB, which is shown to have very good overlaps with these  $\mu$ -conotoxins at the critical binding interface region (Figure 2). We note that the mutagenesis data in Table 1 is mostly consistent with the binding modes suggested in Figure 2. The large affinity changes arising from the mutation of W8 and H12 in KIIIA are most likely due to misfolding of the toxin rather than loss of any interactions with the channel residues. Thus, we perform two docking

calculations for each  $\mu$ -conotoxin, using one of the two pore blocking basic residues identified in Figure 2 and the EEDD ring in Na<sub>v</sub>1.4 as a restraint. The choice of the EEDD ring rather than the DEKA ring is motivated by the fact that the EEDD residues play a much more important role in binding of GIIIA than the DEKA residues [49]. A clustering analysis is performed for the top hundred poses obtained from docking calculations, and a consensus complex is found in each case. Because BuIIIB does not align with GIIIA as well as PIIIA and KIIIA, we have also performed blind docking in this case. The complex obtained from blind docking is found to be consistent with that obtained from restrained docking, confirming that the alignment diagram in Figure 2 is also relevant for the BuIIIB complex.

**Table 1.** Effect of the mutations on the binding affinities of PIIIA and KIIIA to Na<sub>v</sub>1.4. The ratios of the IC<sub>50</sub> values for the mutated (mut) and wild-type (wt) toxins are given in the third column. The binding constants were determined as 249 nM for PIIIA [48] and 82 nM [11], 48 nM [12] and 37 nM [13] for KIIIA.

Residue	Mutation (Mut.)	$\frac{IC_{50} (mut.)}{IC_{50} (wt)}$	Ref.
<b>PIIIA</b>			
R12	A	2.2	[48]
R12	Q	1.6	[48]
R12	K	1.2	[48]
S13	D	6.3	[48]
R14	A	13.0	[48]
R14	Q	15.5	[48]
R14	K	2.2	[48]
K17	A	5.0	[48]
K17	Q	7.0	[48]
H19	Q	0.9	[48]
<b>KIIIA</b>			
K7	A	35.7	[13]
K7	A	13.4	[11]
K7	D	18.3	[11]
W8	R	37.3	[12]
W8	Q	73.2	[12]
W8	E	320	[12]
R10	A	27.1	[13]
H12	A	2986	[13]
R14	A	151	[13]

In the next stage, the Na<sub>v</sub>1.4- $\mu$ -conotoxin complex structure obtained from docking is refined in MD simulations. For this purpose, Nav1.4 in the complex structure is aligned with that embedded in the membrane, and the coordinates of  $\mu$ -conotoxin are transferred to the channel model. Following the protocols established for relaxation of ion channels [50,51], the system is equilibrated in several stages. For details, we refer to [29], where the equilibration procedure and the simulation system for the Na<sub>v</sub>1.4-GIIIA complex was discussed in detail. After equilibration, each Na<sub>v</sub>1.4- $\mu$ -conotoxin complex is simulated for 30 ns to check its stability and to collect data. The trajectory data are then used in the

analysis of the binding modes, where the average distances between strongly interacting pairs of atoms at the binding interface are determined.

### 2.3. MD Simulations and Binding Free Energy Calculations

MD simulations are performed using version 2.7 of NAMD [52] with the CHARMM36 force field [53]. An NpT ensemble is used with periodic boundary conditions. Pressure is kept at 1 atm and temperature at 300 K using Langevin coupling with damping coefficients of  $5 \text{ ps}^{-1}$ . Lennard–Jones interactions are switched off using a smoothing function within a distance of 10–13.5 Å. Electrostatic interactions are calculated using the particle-mesh Ewald algorithm. A time step of 2 fs is employed in MD simulations. The trajectory data is saved at 5-ps intervals, except in umbrella sampling simulations, where the reaction coordinate is saved at every time step.

The binding free energies provide additional means for validation of the complex structures. For this purpose, we construct the potential of mean force (PMF) of the  $\mu$ -conotoxins using umbrella sampling MD simulations, where the toxin is pulled out from the binding pocket to the bulk in small steps. The reaction coordinate is chosen as the distance between the center of mass (COM) of the channel protein and the COM of the toxin along the channel axis. Typically, 30 umbrella windows separated by 0.5 Å are used with a force constant  $k = 30 \text{ kcal/mol/Å}^2$ . Extra windows are inserted if the overlap of densities between two neighboring windows is below 5% or the PMF fails to flatten, which is required to ensure that the bulk region has been reached. The reaction coordinates collected from the simulations are unbiased and combined using the weighted histogram analysis method [54]. Umbrella sampling simulations are continued until the convergence of the PMF is assured from block data analysis of the PMF data.

The binding constant is determined by integrating the PMF,  $W(z)$ , along the  $z$ -axis [33,38]:

$$K_{\text{eq}} = \pi R^2 \int_{z_1}^{z_2} e^{-W(z)/k_B T} dz \quad (1)$$

where  $z_1$  and  $z_2$  are the initial and final points in the PMF and  $\pi R^2$  is the average cross-sectional area of the binding pocket, which is determined from the transverse fluctuations of the COM of the toxin. The value of  $R$ , obtained from restraint-free MD simulations of the  $\text{Na}_V1.4$ -PIIIA complex, is 0.64 Å for PIIIA. The standard binding free energy of the toxin is obtained from the binding constant using:

$$G_b = -k_B T \ln(K_{\text{eq}} C_0) \quad (2)$$

where  $C_0$  is the standard concentration of 1 M. Details of the parameters used in umbrella sampling simulations and justification of the 1D approximation used in the determination of the binding constant are given in [33,38].

## 3. Results and Discussion

### 3.1. Binding Modes of the $\text{Na}_V1.4$ - $\mu$ -Conotoxin Complexes

The docking calculations refined with MD simulations have resulted in fairly unique binding mode for each of the  $\text{Na}_V1.4$ - $\mu$ -conotoxin complexes. Snapshots of the complexes for PIIIA, KIIIA and BuIIIB

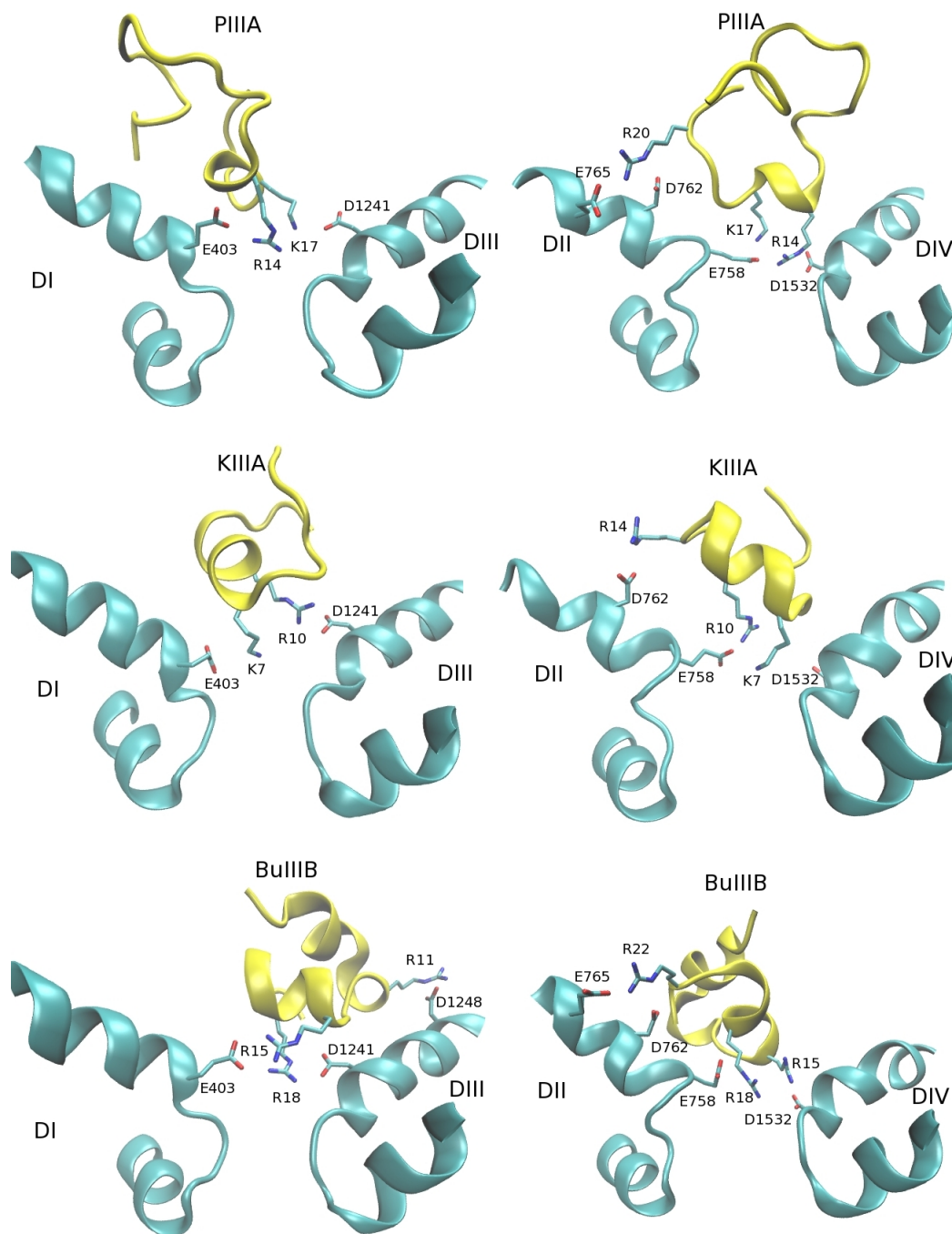
are shown in Figure 3. In each complex, the basic residues corresponding to R13 and K16 in GIIIA (Figures 1 and 2), namely, R14 and K17 in PIIIA, K7 and R10 in KIIIA and R15 and R18 in BuIIIB, are seen to make contacts with the channel residues, E403, E758, D1241 and D1532, forming the EEDD ring. These interactions clearly dominate the binding mode in each complex. It can be seen from Figure 3 that another common interaction occurs between the basic residue corresponding to R19 in GIIIA, that is, R20 in PIIIA, R14 in KIIIA and R22 in BuIIIB, as well as the D762 and D765 residues in DII. Thus, the Na<sub>V</sub>1.4- $\mu$ -conotoxin complexes obtained from docking and MD simulations confirm the presence of a common binding motif, involving the three basic residues identified from the alignment diagrams in Figures 1 and 2.

In order to provide a more quantitative description of the complex structures, which is necessary for a detailed comparison of the binding modes, we present in Table 2 the average N–O distances between strongly interacting pairs. The distances are obtained from 30 ns MD simulations of the complex structures. All of the interacting pairs that have an average distance of 4 Å or less have been included in the table. The results for the Na<sub>V</sub>1.4-GIIIA complex [29] are reproduced here, as they provide a useful reference point for comparison. Most of the contact distances are less than 3 Å, indicating a strong coupling between the N and O atoms. Focusing on the interaction of the PIIIA, KIIIA and BuIIIB residues with the EEDD ring first, it is seen that only two basic residues—those identified in Figure 2—are involved in such interactions. The only other common interaction is in between the D762/E765 residues and the third basic residue identified in the alignment diagram (Figure 1). The comprehensive list of the Na<sub>V</sub>1.4- $\mu$ -conotoxin interactions in Table 2 reinforces the common binding motif proposed from a study of the snapshots in Figure 3.

**Table 2.** List of the interacting residues in the Na<sub>V</sub>1.4- $\mu$ -conotoxin complexes. The average N–O distances obtained from MD simulations are given for each  $\mu$ -conotoxin complex (in units of Å). The acidic residues, E403, E758, D1241 and D1532, forming the EEDD ring, are listed first, as they are responsible for most of the contacts with the  $\mu$ -conotoxin residues. The D762 and E765 residues in DII provide a second anchoring point for a basic  $\mu$ -conotoxin residue and are listed next.

Na <sub>V</sub> 1.4	GIIIA	MD	PIIIA	MD	KIIIA	MD	BuIIIB	MD
E403-O <sub>1</sub>	R13-N <sub>2</sub>	2.7	R14-N <sub>1</sub>	2.7	–	–	R15-N <sub>2</sub>	2.7
E758-O <sub>2</sub>	R13-N <sub>1</sub>	2.8	R14-N <sub>1</sub>	2.7	K7-N <sub>z</sub>	2.9	R18-N <sub>1</sub>	2.7
E758-O <sub>1</sub>	K16-N <sub>z</sub>	2.7	K17-N <sub>z</sub>	2.7	R10-N <sub>1</sub>	2.7	R18-N <sub>2</sub>	3.5
D1241-O <sub>2</sub>	K16-N <sub>z</sub>	2.7	K17-N <sub>z</sub>	2.9	R10-N <sub>2</sub>	2.8	–	–
D1241-O <sub>1</sub>	K11-N <sub>z</sub>	2.7	–	–	–	–	R18-N <sub>2</sub>	2.7
D1532-O <sub>1</sub>	K11-N <sub>z</sub>	2.6	–	–	–	–	–	–
D1532-O <sub>2</sub>	R13-N <sub>2</sub>	2.7	R14-N <sub>E</sub>	2.9	K7-N <sub>z</sub>	3.0	R15-N <sub>2</sub>	2.7
D762-O <sub>2</sub>	R19-N <sub>2</sub>	2.7	R20-N <sub>2</sub>	2.7	R14-N <sub>1</sub>	2.7	R22-N <sub>2</sub>	2.7
E765-O <sub>1</sub>	–	–	–	–	–	–	R22-N <sub>2</sub>	2.7
D1248-O <sub>1</sub>	K8-N <sub>z</sub>	4.0	–	–	–	–	R11-N <sub>2</sub>	2.8

**Figure 3.** Two views of the Na<sub>v</sub>1.4- $\mu$ -conotoxin complexes showing the binding mode for domains I and III (**left**) and II and IV (**right**). All of the important interactions between the channel and toxin residues are indicated explicitly.



It is worthwhile to discuss the binding mode for each  $\mu$ -conotoxin complex in light of the proposed common binding motif. In the GIIIA complex, a third basic residue (K11) is engaged with the EEDD ring, which is not seen in other  $\mu$ -conotoxin complexes. In mutagenesis experiments, K11 is found to have the least impact on binding of GIIIA to Na<sub>v</sub>1.4 compared to the residues, R13, K16 and R19, which form the binding motif [55], confirming its secondary role in the binding mode. Another piece of evidence in this regard comes from alanine mutation of K11, namely, GIIIA[K11A] can still block the channel [55]. The channel is blocked when all four acidic residues in the EEDD ring are engaged with

basic residues of a toxin [28,29]. It is seen from Table 2 that R13 and K16 residues can still cover all four EEDD residues, and hence, K11 is not needed to block the channel.

A similar binding mode is proposed for the Na<sub>V</sub>1.4-GIIIA complex in [28] with one important difference: R19 was assumed to interact with D1532 as an input in modeling, which was retained in the final result. This was motivated by the observation that the residues corresponding to D762 and R395 in Na<sub>V</sub>Ab make a salt bridge, hence D762 and E765 nearby are not likely to be available for binding of R19. However, there is direct evidence from mutagenesis data that substitutions of D762 and E765 affect the binding of GIIIA [55,56]. Furthermore, there are substantial differences between the Na<sub>V</sub>1.4 and Na<sub>V</sub>Ab structures, which make such an assumption questionable. In our MD simulations of Na<sub>V</sub>1.4, we have not observed the formation of such a salt bridge between D762 and R395. Finally, our MD simulations of the Na<sub>V</sub>1.4-GIIIA complex indicate that the EEDD ring region is not wide enough to accommodate four basic residues. This may have been feasible in the Monte Carlo minimization scheme used in [28], which does not take into account entropic contributions. However, when MD simulations are performed at room temperature for such a configuration, the R19 contact is broken, and it is expelled immediately from the EEDD ring region.

PIIIA exhibits the best alignment with GIIIA and has a very similar affinity for Na<sub>V</sub>1.4, e.g., IC<sub>50</sub> values are 19 and 36 nM for GIIIA and PIIIA [6]. (In order to facilitate comparisons, we will use the comprehensive set of  $\mu$ -conotoxin affinities provided in [6]). Thus, from the outset, one would expect very similar binding modes for the two complexes, and this is confirmed by the results shown in Table 2. The only notable difference between the GIIIA and PIIIA complexes is the absence of R12 from the binding mode of PIIIA, which corresponds to K11 in GIIIA. This suggests that the maximum number and type of basic residues that the EEDD ring can accommodate is RKK, as in GIIIA, and replacing one of the K residues with the bulkier R residue in this motif as in PIIIA makes it too crowded to fit in the EEDD ring. The loss of one basic residue from the binding mode should result in some loss of affinity in PIIIA relative to GIIIA, which is in line with the quoted IC<sub>50</sub> values above. The R14 and K17 residues interact with all four EEDD residues (Table 1). Thus, our model predicts blocking of the channel by PIIIA, in agreement with the experimental observations [48].

Our binding mode results for the Na<sub>V</sub>1.4-PIIIA complex again differ from that proposed in [28], where both R12 and R20 were found to make contacts with the EEDD ring. As discussed above for GIIIA, R20 makes contact with the outer D762 residue, and the EEDD ring is not wide enough to accommodate a second arginine on top of R14 and K17, which have established contacts with the EEDD ring. The Na<sub>V</sub>1.4-PIIIA complex was also modeled in [27], where two binding modes with similar binding free energies were proposed. The first involving K9 and R12 is supported neither by the experimental data (Table 1) nor by the arguments based on alignment with GIIIA, which has the best characterized binding mode experimentally. The second binding mode involves R14 and K17, which are fine, but also K9 (instead of R20), which does not occur in our binding mode.

KIIIA is more compact than GIIIA and PIIIA and has only three basic residues. However, it has a good alignment with GIIIA at the binding interface, including the two basic residues (K7 and R10) interacting with the EEDD ring (Figure 2). The main difference is that the RK motif in GIIIA and PIIIA is replaced with KR. Because the lysine side chain is shorter, K7 in that position cannot cover all three domains, leaving E403 free (Table 2). As a result, KIIIA cannot block the channel, in agreement with

the experimental observations [13,57]. Loss of another contact in the binding mode of KIIIA relative to PIIIA is expected to reduce the affinity of KIIIA further, which is consistent with the measured  $IC_{50}$  value of 90 nM [6].

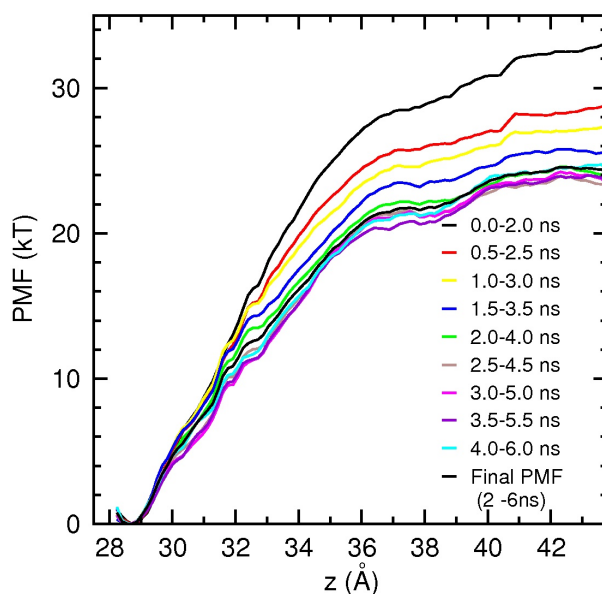
The  $Na_V1.4$ -KIIIA model proposed in [28] has even more substantial differences from ours compared to the those of GIIIA and PIIIA. This is again driven by use of the D1532-R14 interaction as a constraint in modeling, which appears to have displaced K7 from the EEDD ring. As will be shown in the next section, interaction of an arginine residue with D762 is very strong. Sacrifice of D762-R14 in preference for its interaction with the EEDD ring is not justified, especially if this results in loss of a contact for another basic residue (K7).

BuIIIB also has a good alignment with GIIIA at the binding interface with some small differences, e.g., the RK motif in GIIIA and PIIIA is replaced with RR, the third basic residue (R22) is displaced by one residue and K9 and K11 in GIIIA are replaced with R11 and G14. The R15 and R18 residues make contact with all four EEDD residues (Table 2), making sure that BuIIIB blocks the channel, as observed in experiments [32]. Displacement of R22 enables it to make contact with E765 in addition to D762. The D1248-K8 interaction  $Na_V1.4$ -GIIIA is seen to be relatively weak. Thanks to the longer side chain of arginine, the corresponding D1248-R11 interaction in BuIIIB is much stronger. These more than make up for the loss of a basic interaction (K11 in GIIIA) and could explain the higher affinity of BuIIIB relative to GIIIA ( $IC_{50}$  of BuIIIB is 3.6 nM [6]).

### 3.2. Binding Free Energy of PIIIA

Determination of the binding free energies from the PMF calculations is computationally expensive and laborious. Therefore, we present only the results for dissociation of PIIIA from  $Na_V1.4$  here, which provide further validation for the proposed binding motif of  $\mu$ -conotoxins. The PIIIA PMF is constructed using umbrella sampling simulations, as discussed in the ComputationalMethods section. PIIIA has a more stable structure compared to GIIIA, and hence, distortion of the toxin during PMF calculations has not been an issue [29,58]. The results of the PMF calculations are presented in Figure 4. To check the convergence of the results and to separate the production data from equilibration, we perform block data analysis of the data. PMFs are constructed from 2 ns blocks of data to reduce fluctuations, and the blocks are slid in 0.5-ns steps over the collected 6 ns of data. The monotonic drop of the PMFs during the first 2 ns indicates that the system is still equilibrating. After 2 ns, the PMFs fluctuate around the baseline, signaling that the system has been equilibrated. The binding constant is determined by integrating the final PMF in Figure 4 using the prescription in Equation (1), and the binding free energy is obtained from Equation 2 as  $-10.6$  kcal/mol. This is in good agreement with the experimental value of  $-10.2$  kcal/mol [6], providing further validation for the  $Na_V1.4$ -PIIIA model.

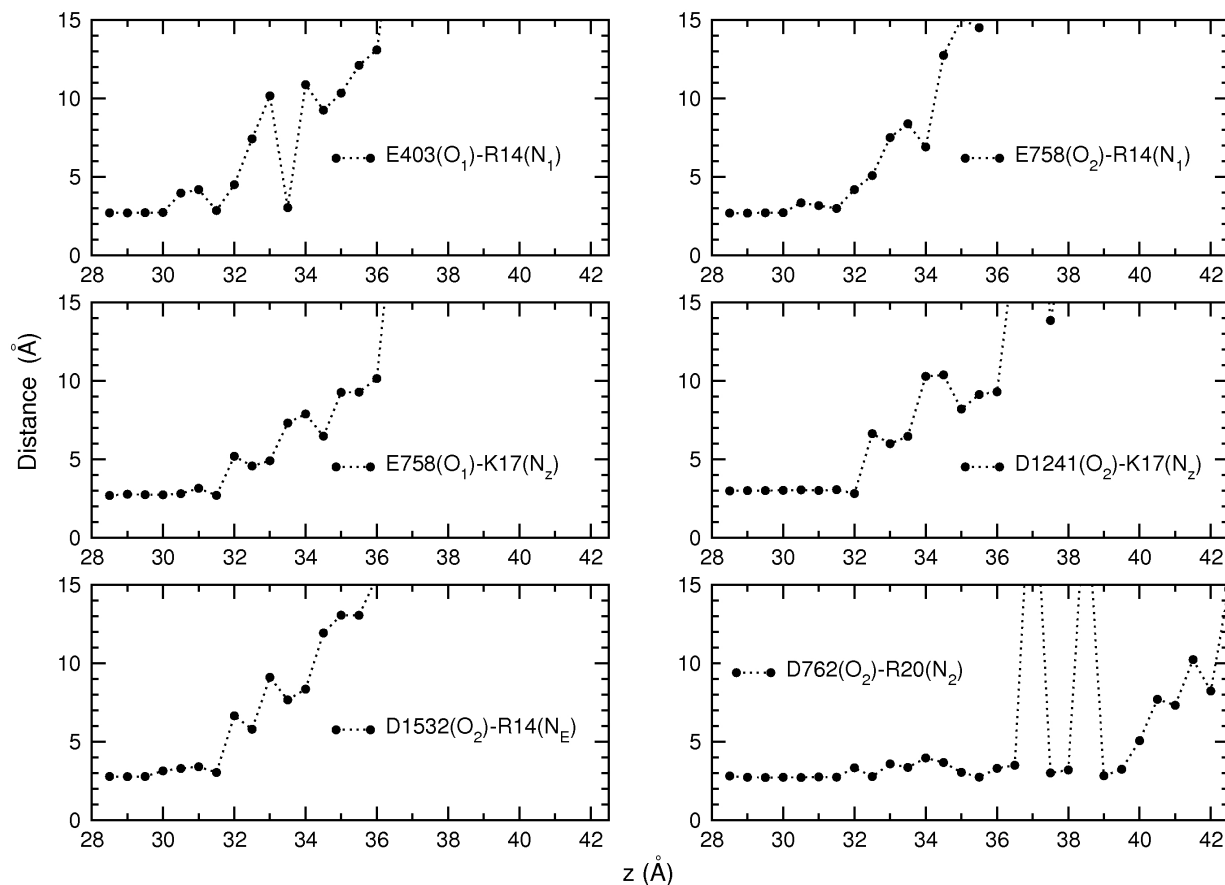
**Figure 4.** Convergence study of the  $\text{Na}_V1.4$ -PIIIA potential of mean force (PMF) from block data analysis. To minimize fluctuations, a large sampling size of 2 ns is used, which is slid in 0.5 ns steps over the available data. The block-data PMFs drop monotonically in the first 2 ns as the system equilibrates and then fluctuate around a baseline, signaling equilibration. The final PMFs obtained from 2 to 6 ns are indicated by a thick black line.



Umbrella sampling simulations provide a wealth of data on the dissociation process, which can be used to gain further insight into the binding mechanism. A very useful quantity in this regard is the persistence length of the interacting pairs, which roughly gives the distance of the toxin from the binding pocket at which a contact is broken. The persistence length is directly related to the interaction strength; hence, it provides complementary information on the relative strength of the individual interactions in a binding mode. To this end, we have calculated the average N–O distance for each pair in Table 2 using the data from each umbrella window. The calculated distances are plotted as a function of the window position in Figure 5. Inspection of the diagrams in Figure 5 shows that the R14 and K17 residues keep their contact with the EEDD ring up to 32 Å, corresponding to a persistence length of 4 Å. The R20 residue keeps contact with D762 up to 36.5 Å, corresponding to a persistence length of over 8 Å. This indicates that the D762-R20 interaction makes a significant contribution to the binding of PIIIA and provides further justification for including the third arginine residue in the common binding motif proposed in the last subsection.

Variation of contact distances can also be used to understand specific features of the PMF. For example, the initial sharp rise in the PMF up to 32 Å is due to stretching of the toxin in order to maintain its charge contacts with the channel residues. Between 32 and 36 Å, R14 and K17 gradually dissociate from EEDD, while the D762-R20 contact persists, resulting in the less steep rise in the PMF. After 36 Å, all of the contacts are broken, and there is only the long-distance Coulomb interaction between the channel and toxin residues. This results in the slowly rising shoulder region in the PMF between 36 and 41 Å. After 41 Å, the Coulomb interactions are also screened, and the PMF becomes flat.

**Figure 5.** Evolution of the distances between the interacting pairs as PIIIA dissociates from Na<sub>V</sub>1.4. Average N–O distances obtained from each umbrella window are plotted as a function of the window position. All of the pairs listed in Table 2 are considered in the figure.



#### 4. Conclusions

We have presented a systematic study of the binding of  $\mu$ -conotoxins to the Na<sub>V</sub>1.4 channel, which revealed a common binding motif for the interaction of  $\mu$ -conotoxins with sodium channels. The binding motif consists of two basic residues (RK or RR) that make contact with the EEDD ring of residues in the pore and a third basic residue (R) that interacts with the higher-lying Asp/Glu residues in domain II (D762/E765 in Na<sub>V</sub>1.4). This is very different from the binding motif found for the toxins that block the potassium channels, which consist of a functional dyad of a pore inserting lysine and an associated aromatic residue, surrounded by a ring of basic residues. Because of the larger vestibule in sodium channels, a single basic residue cannot block the channel. Blocking of the channel is possible when all of the side chains of the EEDD ring are engaged with the basic residues of a toxin, which requires at least two basic residues. As in the case of KIIIA, this may not be enough if the basic residues are not correctly ordered and cannot engage all four EEDD. Another difference from the potassium channels is the lack of tetrameric symmetry. There are few acidic residues in the pore periphery of Na<sub>V</sub>1.4 for anchoring basic residues, e.g., D762/E765 in DII and D1248 in DIII, which is further up and less accessible. Thus, it is not surprising that  $\mu$ -conotoxins have exploited the most available acidic residues in their binding motif.

The binding motifs proposed for GIIIA, PIIIA, KIIIA and BuIIIB provide a general framework for understanding how  $\mu$ -conotoxins interact with sodium channels and will be useful in studies of other  $\mu$ -conotoxins. There are also ongoing efforts for development of drugs from  $\mu$ -conotoxins to treat various diseases associated with dysfunctional sodium channels. The detailed description of the binding modes for the Na<sub>v</sub>1.4- $\mu$ -conotoxin complexes presented here and in [29] will provide valuable guidance in the design of analogs of  $\mu$ -conotoxins with improved affinity and selectivity properties.

### Acknowledgments

This work was supported by a grant from the Australian Research Council. Calculations were performed using the high performance computing facilities at the National Computational Infrastructure (Canberra). We thank Ray Norton for useful discussions on the binding properties of conotoxins.

### Author Contributions

S.M. and S.K. designed the project, analyzed the results and wrote the paper. S.M. performed the simulations in the project.

### Conflicts of Interest

The authors declare no conflict of interest.

### References

1. Hille, B. *Ionic Channels of Excitable Membranes*, 3rd ed.; Sinauer Associates: Sunderland, MA, USA, 2001.
2. Ashcroft, F.M. *Ion Channels and Disease: Channelopathies*; Academic Press: San Diego, CA, USA, 2000.
3. French, R.J.; Terlau, H. Sodium channel toxins—Receptor targeting and therapeutic potential. *Curr. Med. Chem.* **2004**, *11*, 3053–3064.
4. Twede, V.D.; Miljanich, G.; Olivera, B.M.; Bulaj, G. Neuroprotective and cardioprotective conopeptides: An emerging class of drug leads. *Curr. Opin. Drug. Discov. Devel.* **2009**, *12*, 231–239.
5. Norton, R.S.  $\mu$ -Conotoxins as leads in the development of new analgesics. *Molecules* **2010**, *15*, 2825–2844.
6. Wilson, M.J.; Yoshikami, D.; Azam, L.; Gajewiak, J.; Olivera, B.M.; Bulaj, G.; Zhang, M.M.  $\mu$ -Conotoxins that differentially block sodium channels NaV1.1 through 1.8 identify those responsible for action potentials in sciatic nerve. *Proc. Natl. Acad. Sci. USA* **2011**, *108*, 10302–10307.
7. Mantegazza, M.; Curia, G.; Biagini, G.; Ragsdale, D.S.; Avoli, M. Voltage-gated sodium channels as therapeutic targets in epilepsy and other neurological disorders. *Lancet Neurol.* **2010**, *9*, 413–424.

8. Stevens, M.; Peigneur, S.; Dyubankova, N.; Lescrinier, E.; Herdewijn, P.; Tytgat, J. Design of bioactive peptides from naturally occurring  $\mu$ -conotoxin structures. *J. Biol. Chem.* **2012**, *287*, 31382–31392.
9. Lampert, A.; O'Reilly, A.O.; Reeh, P.; Leffler, A. Sodium channelopathies and pain. *Pflug. Arch.* **2010**, *460*, 249–263.
10. Han, T.S.; Zhang, M.M.; Walewska, A.; Gruszczynski, P.; Robertson, C.R.; Cheatham, T.E., III; Yoshikami, D.; Olivera, B.M.; Bulaj, G. Structurally minimized  $\mu$ -conotoxin analogues as sodium channel blockers: implications for designing conopeptide-based therapeutics. *ChemMedChem* **2009**, *4*, 406–414.
11. Zhang, M.M.; Han, T.S.; Olivera, B.M.; Bulaj, G.; Yoshikami, D.  $\mu$ -conotoxin KIIIA derivatives with divergent affinities versus efficacies in blocking voltage-gated sodium channels. *Biochemistry* **2010**, *49*, 4804–4812.
12. Van Der Haegen, A.; Peigneur, S.; Tytgat, J. Importance of position 8 in  $\mu$ -conotoxin KIIIA for voltage-gated sodium channel selectivity. *FEBS J.* **2011**, *278*, 3408–3418.
13. McArthur, J.R.; Singh, G.; McMaster, D.; Winkfein, R.; Tieleman, D.P.; French, R.J. Interactions of key charged residues contributing to selective block of neuronal sodium channels by  $\mu$ -conotoxin KIIIA. *Mol. Pharmacol.* **2011**, *80*, 573–584.
14. Stevens, M.; Peigneur, S.; Dyubankova, N.; Lescrinier, E.; Herdewijn, P.; Tytgat, J. Design of bioactive peptides from naturally occurring  $\mu$ -conotoxin structures. *J. Biol. Chem.* **2012**, *287*, 31382–31392.
15. Khoo, K.K.; Wilson, M.J.; Smith, B.J.; Zhang, M.M.; Gulyas, J.; Yoshikami, D.; Rivier, J.E.; Bulaj, G.; Norton, R.S. Lactam-stabilized helical analogues of the analgesic  $\mu$ -conotoxin KIIIA. *J. Med. Chem.* **2012**, *54*, 7558–7566.
16. Cruz, L.J.; Gray, W.R.; Olivera, B.M.; Zeikus, R.D.; Kerr, L.; Yoshikami, D.; Moczydlowski, D. Conus Geographus toxins that discriminate between neuronal and muscle sodium channels. *J. Biol. Chem.* **1985**, *260*, 9280–9288.
17. Terlau, H.; Olivera, B.M. Conus venoms: A rich source of novel ion channel-targeted peptides. *Physiol. Rev.* **2004**, *84*, 41–68.
18. Li, R.A.; Tomaselli, G.F. Using the deadly  $\mu$ -conotoxins as probes of voltage-gated sodium channels. *Toxicon* **2004**, *44*, 117–122.
19. Dutertre, S.; Lewis, R.J. Use of venom peptides to probe ion channel structure and function. *J. Biol. Chem.* **2010**, *285*, 13315–13320.
20. Payandeh, J.; Scheuer, T.; Zheng, N.; Catterall, W.A. The crystal structure of a voltage-gated sodium channel. *Nature* **2011**, *475*, 353–358.
21. Payandeh, J.; Scheuer, T.; Zheng, N.; Catterall, W.A. Crystal structure of a voltage-gated sodium channel in two potentially inactivated states. *Nature* **2012**, *486*, 135–139.
22. Zhang, X.; Ren, W.; DeCaen, P.; Yan, C.; Tao, X.; Tang, L.; Wang, J.; Hasegawa, K.; Kumasaka, T.; He, J.; *et al.* Crystal structure of an orthologue of the NaChBac voltage-gated sodium channel. *Nature* **2012**, *486*, 130–134.

23. McCusker, E.C.; Bagneris, C.; Naylor, C.E.; Cole, A.R.; D'Avanzo, N.; Nichols, C.G.; Wallace, B.A. Structure of a bacterial voltage-gated sodium channel pore reveals mechanisms of opening and closing. *Nat. Commun.* **2012**, *3*, 1102–1107.
24. Shaya, D.; Findeisen, F.; Abderemane-Ali, F.; Arrigoni, C.; Wong, S.; Nurval, S.R.; Loussouarn, G.; Minor, D.L., Jr. Structure of a prokaryotic sodium channel pore reveals essential gating elements and an outer ion binding site common to eukaryotic channels. *J. Mol. Biol.* **2014**, *426*, 467–483.
25. Tikhonov, D.B.; Zhorov, B.S. Architecture and pore block of eukaryotic voltage-gated sodium channels in view of NavAb bacterial sodium channel structure. *Mol. Pharmacol.* **2012**, *82*, 97–104.
26. Chen, R.; Chung, S.H. Mechanism of tetrodotoxin block and resistance in sodium channels. *Biochem. Biophys. Res. Commun.* **2014**, *446*, 370–374.
27. Chen, R.; Robinson, A.; Chung, S.H. Mechanism of  $\mu$ -conotoxin PIIIA binding to the voltage-gated Na<sup>+</sup> channel Nav1.4. *PLoS One* **2014**, *9*, e93267.
28. Korkosh, V.S.; Zhorov, B.S.; Tikhonov, D.B. Folding similarity of the outer pore region in prokaryotic and eukaryotic sodium channels revealed by docking of conotoxins GIIIA, PIIIA, and KIIIA in a NavAb-based model of Nav1.4. *J. Gen. Physiol.* **2014**, *144*, 231–244.
29. Mahdavi, S.; Kuyucak, S. Molecular dynamics study of binding of  $\mu$ -conotoxin GIIIA to the voltage-gated sodium channel Nav1.4. *PLoS One* **2014**, *9*, e105300.
30. Shon, K.J.; Olivera, B.M.; Watkins, M.; Jacobsen, R.B.; Gray, W.R.; Floresca, C.Z.; Cruz, L.J.; Hillyard, D.R.; Brink, A.; Terlau, H.; *et al.*  $\mu$ -conotoxin PIIIA, a new peptide for discriminating among tetrodotoxin-sensitive Na channel subtypes. *J. Neurosci.* **1998**, *18*, 4473–4481.
31. Bulaj, G.; West, P.J.; Garrett, J.E.; Watkins, M.; Marsh, M.; Zhang, M.M.; Norton, R.S.; Smith, B. J.; Yoshikami, D.; Olivera, B.M. Novel conotoxins from *Conus striatus* and *Conus kinoshitai* selectively block TTX-resistant sodium channels. *Biochemistry* **2005**, *44*, 7259–7265.
32. Holford, M.; Zhang, M.M.; Gowd, K.H.; Azam, L.; Green, B.R.; Watkins, M.; Ownby, J.P.; Yoshikami, D.; Bulaj, G.; Olivera, B.M. Pruning nature: Biodiversity-derived discovery of novel sodium channel blocking conotoxins from *Conus bullatus*. *Toxicon* **2009**, *53*, 90–98.
33. Chen, P.C.; Kuyucak, S. Accurate determination of the binding free energy for KcsA-Charybdotoxin complex from the potential of mean force calculations with restraints. *Biophys. J.* **2011**, *100*, 2466–2474.
34. Chen, P.C.; Kuyucak, S. Developing a comparative docking protocol for the prediction of peptide selectivity profiles: Investigation of potassium channel toxins. *Toxins* **2012**, *4*, 110–138.
35. Rashid, M.H.; Kuyucak, S. Affinity and selectivity of ShK toxin for the Kv1 potassium channels from free energy simulations. *J. Phys. Chem. B* **2012**, *116*, 4812–4822.
36. Rashid, M.H.; Heinzelmann, G.; Huq, R.; Tajhya, R.B.; Chang, S.C.; Chhabra, S.; Pennington, M.W.; Beeton, C.; Norton, R.S.; Kuyucak, S. A potent and selective peptide blocker of the Kv1.3 channel: Prediction from free-energy simulations and experimental confirmation. *PLoS One* **2013**, *8*, e78712.
37. Mahdavi, S.; Kuyucak, S. Why *Drosophila* Shaker K<sup>+</sup> channel is not a good model for ligand binding to voltage-gated Kv1 channels. *Biochemistry* **2013**, *52*, 1631–1640.

38. Rashid, M.H.; Kuyucak, S. Free energy simulations of binding of HsTx1 toxin to Kv1 potassium channels: the basis of Kv1.3/Kv1.1 selectivity. *J. Phys. Chem. B* **2014**, *118*, 707–716.
39. Rashid, M.H.; Huq, R.; Tanner, M.R.; Chhabra, S.; Khoo, K.K.; Estrada, R.; Dhawan, V.; Chauhan, S.; Pennington, M.W.; Beeton, C.; *et al.* A potent and Kv1.3-selective analogue of the scorpion toxin HsTX1 as a potential therapeutic for autoimmune diseases. *Sci. Rep.* **2014**, *4*, 4509. doi:10.1038/srep04509.
40. Tietze, A.A.; Tietze, D.; Ohlensclager, O.; Leipold, E.; Ulrich, F.; Kuhl, T.; Mischo, A.; Buntkowsky, G.; Gorchach, M.; Heinemann, S.H.; Imhof, D. Structurally diverse  $\mu$ -conotoxin PIIIA isomers block sodium channel Nav1.4. *Angew. Chem. Int. Ed.* **2012**, *51*, 4058–4061.
41. Khoo, K.K.; Gupta, K.; Green, B.R.; Zhang, M.M.; Watkins, M.; Olivera, B.M.; Balaram, P.; Yoshikami, D.; Bulaj, G.; Norton, R.S. Distinct disulfide isomers of  $\mu$ -conotoxins KIIIA and KIIIB block voltage-gated sodium channels. *Biochemistry* **2012**, *51*, 9826–9835.
42. Kuang, Z.; Zhang, M.M.; Gupta, K.; Gajewiak, J.; Gulyas, J.; Balaram, P.; Rivier, J.E.; Olivera, B.M.; Yoshikami, D.; Bulaj, G.; *et al.* Mammalian neuronal sodium channel blocker  $\mu$ -conotoxin BuIIIB has a structured N-terminus that influences potency. *ACS Chem. Biol.* **2013**, *8*, 1344–1351.
43. Wakamatsu, K.; Kohda, D.; Hatanaka, H.; Lancelin, J.M.; Ishida, Y.; Oya, M.; Nakamura, H.; Inagaki, F.; Sato, K. Structure-activity relationships of  $\mu$ -conotoxin GIIIA: Structure determination of active and inactive sodium channel blocker peptides by NMR and simulated annealing calculations. *Biochemistry* **1992**, *31*, 12577–12584.
44. Nielsen, K.J.; Watson, M.; Adams, D.J.; Hammarstrom, A.K.; Gage, P.W.; Hill, J.M.; Craik, D.J.; Thomas, L.; Adams, D.; Alewood, P.F.; *et al.* Solution structure of  $\mu$ -conotoxin PIIIA, a preferential inhibitor of persistent tetrodotoxin-sensitive sodium channels. *J. Biol. Chem.* **2002**, *277*, 27247–27255.
45. Khoo, K.K.; Feng, Z.P.; Smith, B.J.; Zhang, M.M.; Yoshikami, D.; Olivera, B.M.; Bulaj, G.; Norton, R.S. Structure of the analgesic  $\mu$ -conotoxin KIIIA and effects on the structure and function of disulfide deletion. *Biochemistry* **2009**, *48*, 1210–1219.
46. Dominguez, C.; Boelens, R.; Bonvin, A.M.J.J. HADDOCK: A protein-protein docking approach based on biochemical or biophysical information. *J. Am. Chem. Soc.* **2003**, *125*, 1731–1737.
47. De Vries, S.J.; van Dijk, A.D.; Krzeminski, M.; van Dijk, M.; Thureau, A.; Hsu, V.; Wassenaar, T.; Bonvin, A.M.J.J. HADDOCK versus HADDOCK: New features and performance of HADDOCK 2.0 on the CAPRI targets. *Proteins* **2007**, *69*, 726–733.
48. McArthur, J.R.; Ostroumov, V.; Al-Sabi, A.; McMaster, D.; French, R.J. Multiple, distributed interactions of  $\mu$ -conotoxin PIIIA associated with broad targeting among voltage-gated sodium channels. *Biochemistry* **2011**, *50*, 116–124.
49. Chahine, M.; Sirois, J.; Marcotte, P.; Chen, L.Q.; Kallen, R.G. Extrapore residues of the S5-S6 loop of domain 2 of the voltage-gated skeletal muscle sodium channel (rSkM1) contribute to the  $\mu$ -conotoxin GIIIA binding site. *Biophys. J.* **1998**, *75*, 236–246.
50. Bastug, T.; Kuyucak, S. Energetics of ion permeation, rejection, binding and block in gramicidin A from free energy simulations. *Biophys. J.* **2006**, *90*, 3941–3950.

51. Bastug, T.; Kuyucak, S. Importance of the peptide backbone description in modeling the selectivity filter in potassium channels. *Biophys. J.* **2009**, *96*, 4006–4012.
52. Phillips, J.C.; Braun, R.; Wang, W.; Gumbart, J.; Tajkhorshid, E.; Villa, E.; Chipot, C.; Skeel, R.D.; Kale, L.; Schulten, K. Scalable molecular dynamics with NAMD. *J. Comput. Chem.* **2005**, *26*, 1781–1802.
53. Vanommeslaeghe, K.; Hatcher, E.; Acharya, C.; Kundu, S.; Zhong, S.; Shim, J.; Darian, E.; Guvench, O.; Lopes, P.; Vorobyov, I.; *et al.* CHARMM general force field: a force field for drug-like molecules compatible with the CHARMM all-atom additive biological force field. *J. Comput. Chem.* **2010**, *31*, 671–690.
54. Kumar, S.; Bouzida, D.; Swensen, R.H.; Kollman, P.A.; Rosenberg, J.M. The weighted histogram analysis method for free-energy calculations on biomolecules. *J. Comput. Chem.* **1992**, *13*, 1011–1021.
55. Xue, T.; Ennis, I.L.; Sato, K.; French, R.J.; Li, R.A. Novel interactions identified between  $\mu$ -conotoxin and the Na<sup>+</sup> channel domain I P-loop: Implications for toxin-pore binding geometry. *Biophys. J.* **2003**, *85*, 2299–2310.
56. Li, R.A.; Ennis, I.L.; French, R.J.; Dudley, S.C., Jr.; Tomaselli, G.F.; Marban, E. Clockwise domain arrangement of the sodium channel revealed by  $\mu$ -conotoxin (GIIIA) docking orientation. *J. Biol. Chem.* **2001**, *276*, 11072–11077.
57. Zhang, M.M.; Green, B.R.; Catlin, P.; Fiedler, B.; Azam, L.; Chadwick, A.; Terlau, H.; McArthur, J.R.; French, R.J.; Gulyas, J.; *et al.* Structure/function characterization of  $\mu$ -conotoxin KIIIA, an analgesic, nearly irreversible blocker of mammalian neuronal sodium channels. *J. Biol. Chem.* **2007**, *282*, 30699–30706.
58. Chen, P.C.; Kuyucak, S. Mechanism and energetics of charybdotoxin unbinding from a potassium channel from molecular dynamics simulations. *Biophys. J.* **2009**, *96*, 2577–2588.